Low-Energy Constants of Chiral Perturbation Theory from Pion Scalar Form Factors in $N_f = 2 + 1$-Flavor Lattice QCD with Controlled Errors

Georg von Hippel* and Konstantin Ottnad†

PRISMA$^+$ Cluster of Excellence and Institut für Kernphysik, Johannes Gutenberg-Universität Mainz, 55099 Mainz, Germany

(Received 2 April 2025; accepted 2 July 2025; published 13 August 2025)

We determine the low-energy constants f_0, L_4^r and L_5^r of SU(3) chiral perturbation theory from a lattice QCD calculation of the scalar form factors of the pion with fully controlled systematics. Lattice results are computed on a large set of $N_f = 2 + 1$ gauge ensembles covering four lattice spacings $a \in [0.049, 0.086]$ fm, pion masses $M_\pi \in [130, 350]$ MeV, and various large physical volumes. By determining the notorious quark-disconnected contributions with unprecedented precision and using a large range of source-sink separations $t_{\text{sep}} \in [1.0, 3.25]$ fm, we are able for the first time to obtain the scalar radii from a z-expansion parametrization of the form factors rather than a simple linear approximation at small momentum transfer. The low-energy constants are obtained from the physical extrapolation of the radii using next-to-leading-order SU(3) next-to-leading-order chiral perturbation theory to parametrize the quark mass dependence. Systematic uncertainties are estimated via model averages based on the Akaike information criterion. Our determination of L_4^r is the first lattice determination to obtain a result not compatible with zero.

DOI: 10.1103/f4x5-frx1

Introduction—Quark-hadron duality implies that one can study low-energy hadron physics via two different approaches, either on the phenomenological level of hadrons using effective theories such as in chiral perturbation theory (χPT), or on the fundamental level of quarks and gluons using nonperturbative quantum chromodynamics (QCD), in particular lattice QCD simulations.

Historically, χPT has been an indispensable tool for lattice QCD practitioners, who required it to extrapolate results from lattice simulations performed using unphysically heavy quark masses to the physical quark mass point. Nowadays, however, the relationship between χPT and lattice QCD has changed, since algorithmic improvements and the progress of computer technology have enabled simulations directly at physical quark masses. Now it is lattice QCD with its ability to simulate at unphysical values of the quark masses that can offer added value to χPT by extracting values for its low-energy constants (LECs) from first principles.

Of particular interest in this context are quantities depending only on a single or very few LECs. An example of such quantities are the scalar radii

$$\langle r_S^2 \rangle_\pi^f = -\frac{6}{F_S^{\pi,f}(0)} \frac{dF_S^{\pi,f}(Q^2)}{dQ^2}\bigg|_{Q^2 \to 0} \tag{1}$$

that parametrize the scalar form factors

$$F_S^{\pi,f}(Q^2) = \langle \pi(\mathbf{p}_f) | \mathcal{S}^f | \pi(\mathbf{p}_i) \rangle \tag{2}$$

at low values of $Q^2 = -q^2 = -(p_f - p_i)^2$. In the $N_f = 2$ theory, the only isoscalar scalar density is the light one,

$$\mathcal{S}^l = \bar{u}u + \bar{d}d, \tag{3}$$

and in SU(2) χPT, the corresponding scalar radius depends only on $\bar{\ell}_4$ via

$$\langle r_S^2 \rangle_\pi^l = \frac{1}{8\pi^2 f_{\pi,\text{phys}}^2} \left[-\frac{13}{2} + \bar{\ell}_4 + \log \frac{M_{\pi,\text{phys}}^2}{M_\pi^2} \right]. \tag{4}$$

With $N_f = 2 + 1$ quark flavors, the scalar densities can be expressed in the basis of the singlet and octet ones,

$$\mathcal{S}^0 = \bar{u}u + \bar{d}d - 2\bar{s}s, \tag{5}$$

$$\mathcal{S}^8 = \bar{u}u + \bar{d}d + \bar{s}s, \tag{6}$$

and in SU(3) χPT, the scalar radii are related by [1]

$$\langle r_S^2 \rangle_\pi^0 = \langle r_S^2 \rangle_\pi^8 + \delta r_S^2, \tag{7}$$

*Contact author: hippel@uni-mainz.de
†Contact author: kottnad@uni-mainz.de

Published by the American Physical Society under the terms of the Creative Commons Attribution 4.0 International license. Further distribution of this work must maintain attribution to the author(s) and the published article's title, journal citation, and DOI. Funded by SCOAP^3.

$$\langle r_S^2\rangle_\pi^l = \langle r_S^2\rangle_\pi^8 + \frac{2}{3}\delta r_S^2, \tag{8}$$

where the octet radius depends only on L_5^r, while the singlet and light radii depend on both L_5^r and L_4^r.

The LECs $\overline{\ell}_4$, and L_5^r and L_4^r can therefore be accurately determined from a high-precision determination of the scalar form factors.

In this Letter, we present a high-statistics determination of the scalar form factors with fully controlled systematics, including the extrapolation to the physical point. The use of moving frames allows us to achieve far better momentum resolution than previous studies, and we determine the numerically challenging quark-disconnected contribution with a statistical precision that is more than an order of magnitude better than the best preceding determination, resulting in the first lattice determination of L_4^r that is not compatible with zero.

For a more detailed description of the technical details of our Letter and the form factors obtained, we refer the reader to the companion paper [2].

Setup—The lattice calculation of the scalar form factors has been carried out on a set of 17 gauge ensembles produced by the Coordinated Lattice Simulations (CLS) consortium [3] using $N_f = 2+1$ flavors of nonperturbatively $\mathcal{O}(a)$-improved Wilson fermions [4] and a tree-level Symanzik-improved gauge action [5]. The majority of the ensembles use open boundary conditions in time to mitigate topological freezing [6,7], whereas some ensembles use periodic boundary conditions. Due to the use of a twisted-mass regulator [7] for the light quarks and a rational approximation for the strange quark [8], reweighting factors [3,9,10] have to be applied when taking gauge averages.

Most of the ensembles lie on the chiral trajectory defined by $\mathrm{tr}[M] = 2m_l + m_s = \mathrm{const}$, but additional ensembles on a second chiral trajectory defined by $m_s \approx m_s^{\mathrm{phys}}$ have been included in order to provide a better handle on the separate m_l and m_s dependence in the chiral extrapolations.

Scale setting is performed via the gradient flow scale t_0 [11], using the values for t_0^{sym}/a^2 at the symmetrical point from Ref. [12], while defining the physical light and strange quark masses using the $N_f = 2+1$ flavour lattice averaging group (FLAG) world average [13]

$$\sqrt{t_0^{\mathrm{phys}}} = 0.14464(87)\ \mathrm{fm}, \tag{9}$$

The matrix elements in Eq. (2) are evaluated in lattice QCD by taking the ratio

$$R^f(\mathfrak{p}_f, \mathfrak{q}, \mathfrak{p}_i, t_{\mathrm{sep}}, t_{\mathrm{ins}}) = \frac{\langle C^{3\mathrm{pt}}_{P\mathcal{S}^f P}(\mathfrak{p}_f, \mathfrak{q}, \mathfrak{p}_i, t_{\mathrm{sep}}, t_{\mathrm{ins}})\rangle}{\langle C^{2\mathrm{pt}}_{PP}(\mathfrak{p}_f, t_{\mathrm{sep}})\rangle} \sqrt{\frac{\langle C^{2\mathrm{pt}}_{PP}(\mathfrak{p}_i, t_{\mathrm{sep}}-t_{\mathrm{ins}})\rangle\langle C^{2\mathrm{pt}}_{PP}(\mathfrak{p}_f^2, t_{\mathrm{ins}})\rangle\langle C^{2\mathrm{pt}}_{PP}(\mathfrak{p}_f^2, t_{\mathrm{sep}})\rangle}{\langle C^{2\mathrm{pt}}_{PP}(\mathfrak{p}_f^2, t_{\mathrm{sep}}-t_{\mathrm{ins}})\rangle\langle C^{2\mathrm{pt}}_{PP}(\mathfrak{p}_i^2, t_{\mathrm{ins}})\rangle\langle C^{2\mathrm{pt}}_{PP}(\mathfrak{p}_i^2, t_{\mathrm{sep}})\rangle}}, \tag{10}$$

of the two- and three-point functions

$$C^{2\mathrm{pt}}_{PP}(\mathbf{p}, t) = \sum_{\mathbf{x}_f} e^{i\mathbf{p}\cdot\mathbf{x}_f}\langle P(\mathbf{x}_f, t)P^\dagger(\mathbf{0}, 0)\rangle_F, \tag{11}$$

$$C^{3\mathrm{pt}}_{P\mathcal{S}^f P}(\mathbf{p}_f, \mathbf{q}, t_{\mathrm{sep}}, t_{\mathrm{ins}}) = \sum_{\mathbf{x}_f, \mathbf{x}_{\mathrm{op}}} e^{i\mathbf{p}_f\cdot\mathbf{x}_f} e^{i\mathbf{q}\cdot\mathbf{x}_{\mathrm{op}}}\langle P(\mathbf{x}_f, t_{\mathrm{sep}})\mathcal{S}^f(\mathbf{x}_{\mathrm{op}}, t_{\mathrm{ins}})P^\dagger(\mathbf{0}, 0)\rangle_F, \tag{12}$$

where $P(\mathbf{x}, t) = (1/\sqrt{2})[\bar{u}\gamma_5 u + \bar{d}\gamma_5 d](\mathbf{x}, t)$, and $(\mathfrak{p}_f, \mathfrak{q}, \mathfrak{p}_i)$ are equivalence classes of lattice momenta $(\mathbf{p}_f, \mathbf{q}, \mathbf{p}_i)$ over which the correlation functions have been averaged.

Performing the Wick contractions for the fermionic expectation value $\langle\cdot\rangle_F$ in the three-point function in Eq. (12) yields both quark-connected and quark-disconnected diagrams. The quark-connected piece is computed to high statistical precision using a sequential propagator through the sink [14] and the truncated solver method [15–17]. The numerical evaluation of the quark-disconnected contribution requires correlating two-point functions $C^{2\mathrm{pt}}_{PP}(\mathbf{p}_f, t)$ with scalar quark loops,

$$L_{\mathcal{S}^f}(\mathbf{q}, t) = -\sum_{\mathbf{x}} e^{i\mathbf{q}\cdot\mathbf{x}}\mathrm{tr}\left[D_f^{-1}(x, x)\right], \tag{13}$$

where D_f is the Dirac operator for quark flavor $f = l, s$. These loops have been calculated using the (OET + gHPE + HP) prescription we introduced in Ref. [18] on the basis of the method of Ref. [19], combining the one-end trick (OET) [20] with the generalized hopping parameter expansion (gHPE) [21] and hierarchical probing (HP) [22].

One final wrinkle concerns the estimation of the subtraction of the vacuum expectation value of the scalar loop at zero momentum. With open boundary conditions, the need to avoid the region close to the boundaries leads to restrictions on the source positions that can be used at a given t_{sep}, which in turn leads to an amplification of fluctuations in the loop at large t_{sep}, where few sources contribute to the two-point function. To cancel these fluctuations, we determine and subtract the vacuum expectation value on each time slice separately, leading to a large

improvement in signal quality. For technical details, cf. Ref. [2].

Data analysis—For large time separations, the ratio (10) tends directly to the scalar form factor of the pion, $\lim_{t_{\rm sep}\gg t_{\rm ins}\to\infty} R^f(\mathfrak{p}_f,\mathfrak{q},\mathfrak{p}_i,t_{\rm sep},t_{\rm ins}) = F_S^{\pi,f}(Q^2)$. To extract the form factor at finite $t_{\rm sep}$, $t_{\rm ins}$, we use the summation method [23–26]

$$\sum_{t_{\rm ins}=\tau}^{t_{\rm sep}-\tau} R^f(\mathfrak{p}_f,\mathfrak{q},\mathfrak{p}_i,t_{\rm sep},t_{\rm ins}) = C_\tau + t_{\rm sep} F_S^{\pi,f}(Q^2) + \mathcal{O}(e^{-\Delta t_{\rm sep}}), \tag{14}$$

where C_τ is an irrelevant constant, and Δ is the energy gap between the first excited state and the ground state. We perform linear fits over different ranges $t_{\rm sep}\in[t_{\rm sep}^{\rm min}, t_{\rm sep}^{\rm max}]$ of the summed ratio, where $1.0\ {\rm fm} \lesssim t_{\rm sep}^{\rm min} \lesssim 1.5\ {\rm fm}$ and $2.5\ {\rm fm} \lesssim t_{\rm sep}^{\rm max} \lesssim 3.0\ {\rm fm}$ on each ensemble, and $\tau = t_{\rm sep}^{\rm min}/2$.

We parametrize the Q^2 dependence of the resulting form factors using the z-expansion ansatz

$$F_S^{\pi,f}(Q^2) = \sum_{n=0}^{N_z} a_n z^n, \quad z = \frac{\sqrt{t_{\rm cut}+Q^2}-\sqrt{t_{\rm cut}-t_{\rm opt}}}{\sqrt{t_{\rm cut}+Q^2}+\sqrt{t_{\rm cut}-t_{\rm opt}}}, \tag{15}$$

in terms of which the radii are given by

$$a_1 \sim \langle r_S^2\rangle_\pi^f = -\frac{6}{F_S^{\pi,f}(0)} \cdot \left.\frac{dF_S^{\pi,f}(Q^2)}{dQ^2}\right|_{Q^2=0}. \tag{16}$$

In our fits, which we perform for five different cuts $Q^2_{\rm max}\in[0.2, 0.4]\ {\rm GeV}^2$ on $Q^2 \le Q^2_{\rm max}$, we always use $N_z = 1$, $t_{\rm cut} = 4M_\pi^2$, and $t_{\rm opt} = t_{\rm cut}(1-\sqrt{1+Q^2_{\rm max}/t_{\rm cut}})$ [27].

Examples of the form factors obtained are shown in Fig. 1. It can be clearly seen that the addition of moving frames greatly improves the precision of the data and allows fits out to much larger momentum transfers.

To extrapolate the scalar radii to the physical point, we use fit *Ansätze* based on next-to-leading-order $SU(3)$ χPT. To this end, we rewrite the expressions for $\langle r_S^2\rangle_\pi^8$ and δr_S^2 in terms of the leading-order quark-mass proxies $\xi_l = t_0 M_\pi^2$ and $\xi_s = t_0(2M_K^2 - M_\pi^2)$, expressing all dimensionful observables in units of t_0 such that the scale dependence μ is absorbed in the definitions of $L^r_{4,5}$, implicitly setting $\sqrt{t_0}\mu = 1$ in the fits. We also include a term $\sim a^2/t_0$ to account for discretization effects. To account for finite-volume effects, we have also included the finite-volume corrections [28], but found that these tend to worsen the fit quality while having no significant impact on the central values due to our already rather large volumes.

While simultaneous fits for all three radii would in principle allow simultaneous access to all LECs, we find that the very strong correlations between the different radii render such fits problematic, resulting in typically unacceptable fit qualities. We therefore opt to fit suitable linear combinations that isolate L_4^r and L_5^r.

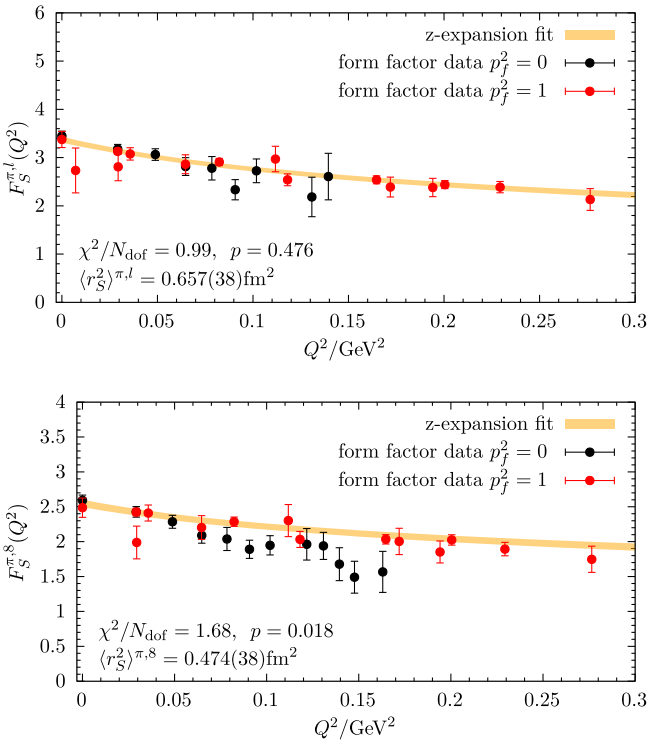


FIG. 1. Form factor data (black for $\mathbf{p}_f{}^2 = 0$ and red for $\mathbf{p}_f{}^2 = 1$ frame) and z-expansion fit bands for $F_S^{\pi,l}(Q^2)$ (top) and $F_S^{\pi,8}(Q^2)$ (bottom) on the physical-mass ensemble E250. The results shown are for the dataset with source-sink separations $t_{\rm sep}\in[1.25, 3.25]$ fm in the summation method, and a fit range $Q^2 \le 0.3\ {\rm GeV}^2$ for the z expansion.

We perform the entire analysis chain with different cuts on the range of $t_{\rm sep}$ used in the summation method, the range of Q^2 fitted in the z-expansion fit, and the values of a, M_π, and $M_\pi L$ included in the physical extrapolation. To arrive at our final best estimates including the full statistical and systematic errors, we perform a model average [29,30] based on the Akaike information criterion [31,32] by computing weights

$$w_{n,b} = \frac{e^{-B_{n,b}}}{N_B \sum_{k=1}^{N_M} e^{-B_{k,b}}} \tag{17}$$

for model $n\in\{1,\ldots N_M\}$ on bootstrap resample $b\in\{1,\ldots,N_B\}$ with

$$B_{n,b} = \frac{1}{2}\chi^2_{n,b} + N_{{\rm par},n} + N_{{\rm cut},n} - N_{\rm prio}, \tag{18}$$

where $\chi^2_{n,b}$ is the correlated χ^2 for model n on bootstrap resample b, and $N_{{\rm par},n}$ and $N_{{\rm cut},n}$ are the number of parameters in model n and the number of data points cut for fitting with model n, respectively [32], while

$N_{\text{prio}} = 1$ accounts for the (uninformative) prior applied to f_0 to stabilize the fits. Our empirical cumulative distribution function (CDF) is then

$$\text{CDF}(x) = \sum_{b=1}^{N_B} \sum_{n=1}^{N_M} w_{n,b} \Theta(x - x_{n,b}), \tag{19}$$

where $x_{n,b}$ is the value of x obtained from model n on bootstrap sample b, and Θ is the Heaviside step function.

Our final results for the LECs of SU(3) χPT are

$$f_0 = 116.5(5.5)_{\text{stat}}(13.7)_{\text{sys}}[14.8]_{\text{total}}\ \text{MeV}, \tag{20}$$

$$L_4^r(\mu) = +0.38(09)_{\text{stat}}(15)_{\text{sys}}[18]_{\text{total}} \times 10^{-3}, \tag{21}$$

$$L_5^r(\mu) = +0.58(0.38)_{\text{stat}}(1.08)_{\text{sys}}[1.14]_{\text{total}} \times 10^{-3}, \tag{22}$$

with the scale-dependent L_i^r evaluated at a renormalization scale of $\mu = 770$ MeV. The corresponding CDFs are shown in the first three panels of Fig. 2.

For the leading-order LEC f_0, our result is in excellent agreement with the FLAG [13,33] estimate $f_0 = 113.6(8.5)$ MeV, albeit with slightly larger errors. We note that the FLAG estimate derives essentially from a single calculation of pion and kaon decay constants (not a form factor calculation). We also agree almost perfectly with the recent semiphenomenological estimate [34] $f_0 = 116.46(96)$ MeV and within the respective errors with the RQCD Collaboration result [35] $f_0 = 99^{+4}_{-3}$ MeV, while being in some tension with the result [36] of $f_0 = 82.3(14.1)$ MeV from the spectrum of the overlap Dirac operator. For the next-to-leading-order LEC L_4^r, our result is the first lattice result not to be compatible with zero, to be compared with the FLAG estimate [13,33] $L_4^r(\mu) = -0.02(56) \times 10^{-3}$. On the other hand, our form factor analysis is not able to obtain a sufficiently precise value for L_5^r, where the FLAG estimate [13,33] $L_5^r(\mu) = +0.95(41) \times 10^{-3}$ based on an analysis of pion and kaon decay constants remains more accurate.

Fitting the SU(2) χPT formula to the results for the light scalar radius, we obtain, for the corresponding LEC,

$$\bar{\ell}_4 = 3.99(15)_{\text{stat}}(17)_{\text{sys}}[23]_{\text{total}}, \tag{23}$$

in perfect agreement with, and about half the total error of, the FLAG [13,33,37–40] estimate $\bar{\ell}_4 = 4.02(45)$.

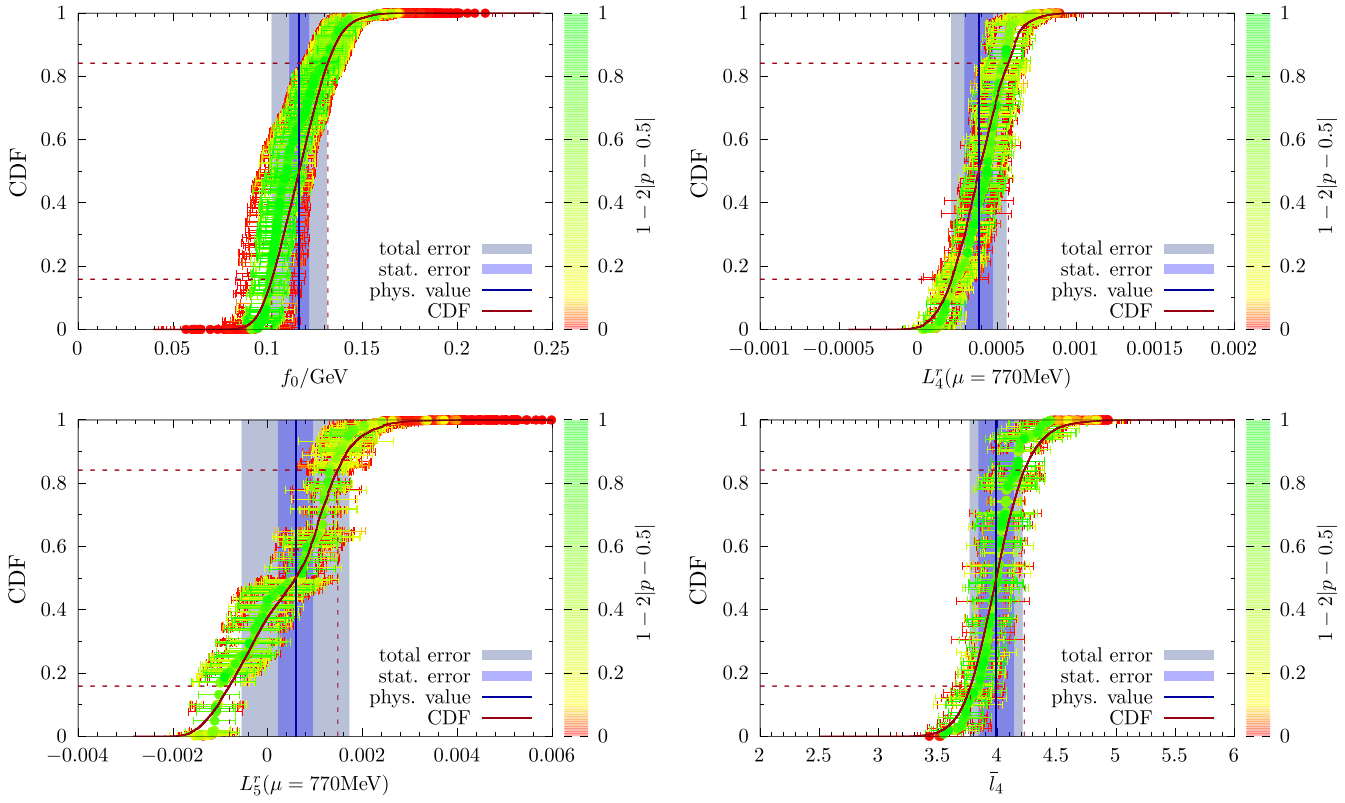


FIG. 2. Cumulative distribution functions (CDFs) of the results for the SU(3) LECs f_0, $L_4^r(\mu)$ and $L_5^r(\mu)$ at a scale of $\mu = 770$ MeV and the SU(2) LEC $\bar{\ell}_4$. Each data point represents the result and statistical error from an individual fit model and its color is determined by the corresponding p value indicating the quality of the fit (which is different from the Akaike weight actually used to obtain the CDF). The solid vertical line indicates the final result from the model average, with the shaded bands giving its statistical and full errors, and the dashed lines corresponding to the 1σ quantiles of the CDF.

The corresponding CDF is shown in the last panel of Fig. 2.

Summary and discussion—We have obtained lattice results for the scalar form factors of the pion that extend over a larger momentum range and have a much higher precision than any previous study. As a result, we have been able to obtain the corresponding LECs of SU(2) and SU(3) χPT with fully controlled errors, being able for the first time to give an estimate for L_4^r that is not compatible with zero.

We note that all existing determinations of SU(3) LECs as well as the determinations of $\overline{\ell}_4$ using $N_f = 2 + 1$ quark flavors are based on decay constants, and thus involve two-point functions only, whereas we present the first form factor calculation for $N_f = 2 + 1$.

The LEC L_4^r, which we have been clearly able to distinguish from zero, notably parametrizes a strange quark effect given by a purely quark-disconnected contribution, that can be very cleanly determined from, e.g., $\langle r_S^2\rangle_\pi^0 - \langle r_S^2\rangle_\pi^l$ in our calculation, yielding a clear advantage for a form factor calculation.

For L_5^r on the other hand, our analysis does not have the same impact due to, somewhat paradoxically, the high statistical precision to which the octet radius determining it is computed: this leads to a large number of poor model fits and a somewhat skewed CDF, in which the systematic error absolutely dominates.

A more detailed description of our Letter and the form factors obtained can be found in the companion paper [2].

Acknowledgments—The authors thank Stephan Dürr and Andreas Jüttner for useful comments and discussions. This research is supported by the Deutsche Forschungsgemeinschaft (DFG, German Research Foundation) through Project No. HI 2048/1-3 (Project No. 399400745). The authors gratefully acknowledge the Gauss Centre for Supercomputing e.V. (www.gauss-centre.eu) for funding this project by providing computing time on the GCS Supercomputer SuperMUC-NG at Leibniz Supercomputing Centre and on the GCS Supercomputers JUQUEEN [41] and JUWELS [42] at Jülich Supercomputing Centre (JSC). The authors gratefully acknowledge the computing time made available to them on the high-performance computer Mogon-NHR at the NHR Centre NHR Süd-West. This center is jointly supported by the Federal Ministry of Education and Research and the state governments participating in the NHR (www.nhr-verein.de/unsere-partner). Additional calculations have been performed on the HPC clusters Clover at the Helmholtz-Institut Mainz and Mogon II and HIMster-2 at Johannes-Gutenberg Universität Mainz. The QDP ++ library [43] and the deflated SAP + GCR solver from the OPENQCD package [44] have been used in our simulation code. We thank our colleagues in the CLS initiative for sharing gauge ensembles.

Data availability—The data that support the findings of this article are not publicly available upon publication because it is not technically feasible and/or the cost of preparing, depositing, and hosting the data would be prohibitive within the terms of this research project. The data are available from the authors upon reasonable request.

[1] J. Gasser and H. Leutwyler, Nucl. Phys. **B250**, 517 (1985).
[2] K. Ottnad and G. von Hippel, companion paper, Phys. Rev. D **112**, 034504 (2025).
[3] M. Bruno *et al.*, J. High Energy Phys. 02 (2015) 043.
[4] B. Sheikholeslami and R. Wohlert, Nucl. Phys. **B259**, 572 (1985).
[5] M. Lüscher and P. Weisz, Commun. Math. Phys. **98**, 433 (1985); **98**, 433(E) (1985)].
[6] M. Lüscher and S. Schaefer, J. High Energy Phys. 07 (2011) 036.
[7] M. Lüscher and S. Schaefer, Comput. Phys. Commun. **184**, 519 (2013).
[8] M. A. Clark and A. D. Kennedy, Phys. Rev. Lett. **98**, 051601 (2007).
[9] S. Kuberski, Comput. Phys. Commun. **300**, 109173 (2024).
[10] D. Mohler and S. Schaefer, Phys. Rev. D **102**, 074506 (2020).
[11] M. Lüscher, J. High Energy Phys. 08 (2010) 071; 03 (2014) 92(E).
[12] M. Bruno, T. Korzec, and S. Schaefer, Phys. Rev. D **95**, 074504 (2017).
[13] Y. Aoki *et al.* (Flavour Lattice Averaging Group (FLAG)), Eur. Phys. J. C **82**, 869 (2022).
[14] D. Dolgov *et al.* (LHPC Collaboration and TXL Collaboration), Phys. Rev. D **66**, 034506 (2002).
[15] G. S. Bali, S. Collins, and A. Schäfer, Comput. Phys. Commun. **181**, 1570 (2010).
[16] T. Blum, T. Izubuchi, and E. Shintani, Phys. Rev. D **88**, 094503 (2013).
[17] E. Shintani, R. Arthur, T. Blum, T. Izubuchi, C. Jung, and C. Lehner, Phys. Rev. D **91**, 114511 (2015).
[18] M. Cè *et al.*, J. High Energy Phys. 08 (2022) 220.
[19] L. Giusti, T. Harris, A. Nada, and S. Schaefer, Eur. Phys. J. C **79**, 586 (2019).
[20] C. McNeile and C. Michael (UKQCD Collaboration), Phys. Rev. D **73**, 074506 (2006).
[21] V. Gülpers, G. von Hippel, and H. Wittig, Phys. Rev. D **89**, 094503 (2014).
[22] A. Stathopoulos, J. Laeuchli, and K. Orginos, SIAM J. Sci. Comput. **35**, S299 (2013).
[23] L. Maiani, G. Martinelli, M. L. Paciello, and B. Taglienti, Nucl. Phys. **B293**, 420 (1987).
[24] S. Güsken, U. Löw, K.-H. Mütter, R. Sommer, A. Patel, and K. Schilling, Phys. Lett. B **227**, 266 (1989).
[25] J. Bulava, M. Donnellan, and R. Sommer, J. High Energy Phys. 01 (2012) 140.
[26] S. Capitani, M. Della Morte, G. von Hippel, B. Jäger, A. Jüttner, B. Knippschild, H. B. Meyer, and H. Wittig, Phys. Rev. D **86**, 074502 (2012).
[27] G. Lee, J. R. Arrington, and R. J. Hill, Phys. Rev. D **92**, 013013 (2015).

[28] G. Colangelo, S. Dürr, and C. Haefeli, Nucl. Phys. **B721**, 136 (2005).
[29] K. P. Burnham and D. R. Anderson, Sociol. Methods Res. **33**, 261 (2004).
[30] S. Borsányi *et al.* (BMW Collaboration), Science **347**, 1452 (2015).
[31] H. Akaike, IEEE Trans. Autom. Control **19**, 716 (1974).
[32] E. T. Neil and J. W. Sitison, Phys. Rev. D **109**, 014510 (2024).
[33] A. Bazavov *et al.* (MILC Collaboration), Proc. Sci., LATTICE2010 (**2010**) 074 [arXiv:1012.0868].
[34] M. F. M. Lutz, Y. Heo, and R. J. Hudspith, Phys. Rev. D **110**, 094046 (2024).
[35] G. S. Bali, S. Collins, W. Söldner, and S. Weishäupl (RQCD Collaboration), Phys. Rev. D **105**, 054516 (2022).
[36] J. Liang, A. Alexandru, Y. J. Bi, T. Draper, K. F. Liu, and Y. B. Yang (χQCD Collaboration), Phys. Rev. D **110**, 094513 (2024).
[37] S. R. Beane, W. Detmold, P. M. Junnarkar, T. C. Luu, K. Orginos, A. Parreño, M. J. Savage, A. Torok, and A. Walker-Loud, Phys. Rev. D **86**, 094509 (2012).
[38] S. Borsányi, S. Dürr, Z. Fodor, S. Krieg, A. Schäfer, E. E. Scholz, and K. K. Szabó, Phys. Rev. D **88**, 014513 (2013).
[39] S. Dürr *et al.* (BMW Collaboration), Phys. Rev. D **90**, 114504 (2014).
[40] P. A. Boyle *et al.*, Phys. Rev. D **93**, 054502 (2016).
[41] Jülich Supercomputing Centre, J. Large-Scale Res. Facil. **1**, A1 (2015).
[42] Jülich Supercomputing Centre, J. Large-Scale Res. Facil. **7**, A138 (2021).
[43] R. G. Edwards and B. Joo (SciDAC Collaboration, LHPC Collaboration, and UKQCD Collaboration), Nucl. Phys. B, Proc. Suppl. **140**, 832 (2005).
[44] M. Lüscher *et al.*, OPENQCD, http://luscher.web.cern.ch/luscher/openQCD/.